Characteristics of Diurnal Variations in Convection and Precipitation over the Southern Tibetan Plateau during Summer

Hatsuki Fujinami[†1], Shigeyuki Nomura[2] and Tetsuzo Yasunari[3]
[1]*Japan Science and Technology Agency, Kawaguchi, Japan*
[2]*Japan Weather Association, Tokyo, Japan*
[3]*Hydrospheric Atmospheric Research Center, Nagoya University, Nagoya, Japan*

Abstract

This study investigated diurnal cycles in convection and precipitation over the complex mountain-valley terrain of the southern Tibetan Plateau (TP) during the mature phase of the summer monsoon. Cloud-cover frequency (CCF) for high cloud increased after 13 LST (07 UTC) over the mountain ranges along 28.5°N and 30.2°N, reaching a maximum near 18 LST (12 UTC). Areas of high CCF subsequently moved towards the valley area along 29.3°N; relatively high CCF persisted there until early morning. Tropical Rainfall Measuring Mission (TRMM) PR data show a nearly identical variation in rainfall frequency. Formation and development of convective-type clouds and phase differences in the diurnal cycle were strongly affected by TP topography. Possible mechanisms for convective enhancement over the southern TP are also discussed.

1. Introduction

Diurnal variation of convection is a notable phenomenon over the Tibetan Plateau (TP) during the summer (e.g., Murakami 1983; Fujinami and Yasunari 2001). Convective activity over the TP is a major heat source in the Asian monsoon region (e.g., Yanai et al. 1992; Ueda et al. 2003). Yanai and Li (1994) noted that a vertical circulation and associated convective activity over and around the TP in the summer are maintained by a thermally induced plateau-scale circulation that is driven by thermal contrasts between the plateau and surrounding regions. Sasaki et al. (2003) used results from a numerical model and showed that diurnal variations in precipitable water (PW) at Lhasa (29.7°N, 91.1°E) in October were associated with a plateau-scale diurnal circulation system. Recent studies have discussed the relationship between convection (or precipitation) and topography over the TP during summer. Ueno (1998) showed that satellite-estimated precipitation is more likely to be over the major mountain ranges during the day (06–18 LST at 90°E) and over major valleys at night (18–06 LST). Kurosaki and Kimura (2002) used Geostationary Meteorological Satellite (GMS) visible and infrared data for both pre-monsoon and monsoon periods in 1998 to show that daytime (09–15 LST) clouds prevail over major mountain ranges of the TP. Such variations could be related to thermally induced local circulations driven by the topography of the TP. The major mountain ridges and valleys of the TP are aligned east-west (c.f., Fig. 1a), and valleys are 100–300 km wide; Kuwagata et al. (2001) used a numerical model to show that this width is a very effective topographic scale for transport of water vapor by thermally induced circulation during the summer. They also noted that the diurnal cycle of PW over the TP results from water vapor transport by the local circulation.

Past studies have not investigated the complete diurnal cycle in convection and precipitation during the mature phase of the monsoon. The present study examines diurnal characteristics, such as the transition from noon to midnight, over the complex mountain-valley terrain of the southern TP. The study focuses on August when a maximum in local convection over the southern TP appears in the seasonal cycle (Fujinami and Yasunari 2001). Clarifying this diurnal cycle over the southern TP will yield information on the water cycle for this region of active convection.

2. Data

This study used hourly GMS-IR equivalent blackbody temperature (Tbb) data on a 0.05° × 0.05° grid as a proxy for cloudiness. High clouds suggest strong convection, and they were inferred from the cloud index *Ic*: *Ic* = 230-Tbb(K) if 230-Tbb(K) > 0; *Ic* = 0 if 230-Tbb < 0. Reanalysis data from the Global Energy and Water Cycle Experiment-Asian Monsoon Experiment (GAME) show that the 230-K threshold is the air temperature about 12 km above sea level over the southern TP. Cloud-cover frequency (CCF) is the percentage of cloud cover (*Ic* > 0) times the total number of available data points in each grid at each hour. Tropical Rainfall Measuring Mission (TRMM) precipitation radar (PR) data (product 2A25) diagnosed the diurnal precipitation cycle. PR algorithm version 5 was used. Rain types considered were convective, stratiform, and other (Awaka et al. 1997). Rainfall frequency (RF) for each 0.05° × 0.05°-grid was determined from the number of rainfall events relative to the total number of samples. A rain flag marked the occurrence of rain. Version 1.5 GAME reanalysis data, on a 0.5° × 0.5°-grid, diagnosed atmospheric circulations (Yamazaki et al. 2000; Ueda et al. 2003). The present study examined Tbb and GAME reanalysis data for August 1998. Five years (1998–2002) of TRMM PR data for August reduced any sampling bias that could arise because of the non-sun-synchronous orbit of TRMM.

3. Results

Figure 1a shows the topography of the central and southern TP. Dotted lines A and B indicate major valleys (unnamed and Yarlung-Zangbo River). Short dashed lines C and D denote major mountain ranges (Nyainqentanglha Range and the northern Himalayas). Valleys A and B have meridional widths of ~300 km

[†]Corresponding author: Hydrospheric Atmospheric Research Center, Nagoya University, Nagoya 464-8601, Japan. E-mail: hatsuki@hyarc.nagoya-u.ac.jp

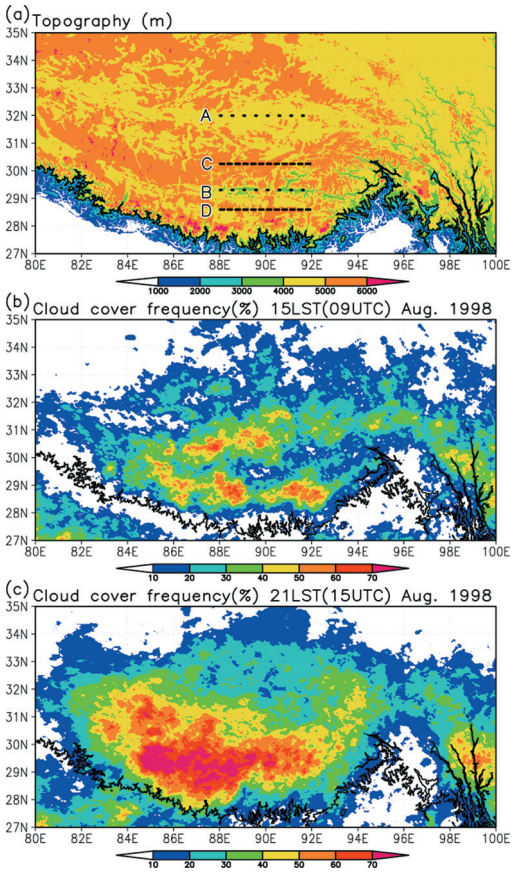

Fig. 1. (a) Tibetan Plateau topography. The solid line is the 3000-m topographic contour. Dotted lines indicate major valleys A (unnamed) and B (Yarlung-Zangbo River). Dashed lines indicate major mountain ranges C (including Nyainqentanglha Range) and D (northern part of the Himalayas). (b) Average distribution of cloud-cover frequency at 15 LST for August 1998. (c) As in (b) but for 21 LST.

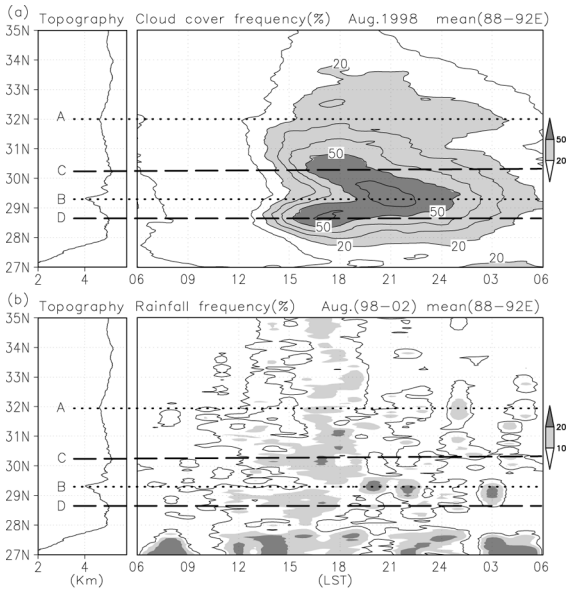

Fig. 2. (a) Latitude-Time section of cloud-cover frequency averaged between 88° and 92°E for August 1998. Contour interval is 10%. The left-hand figure shows surface altitude averaged over the same longitudes. (b) As in (a) but for rainfall frequency averaged for five Augusts (1998–2002). The solid line denotes the 5% contour.

and ~150 km, respectively; they have average depths of ~500 m and ~1000 m along each dotted line between 88°–92°E. Figure 1b shows the distribution of CCF at 15 LST (09 UTC) for August 1998. Zonally elongated regions of high CCF are found near 28.5°N and 30.2°N, close to major mountain ranges C and D. High clouds are suppressed over valley B at 29.3°N. The CCF distribution is consistent with that shown by Kurosaki and Kimura (2002). At 21 LST (Fig. 1c), in contrast, the highest CCF values are over a wide region centered on valley B. The greatest difference in CCF between 15 LST and 21 LST is over valley B.

Figure 2a shows a latitude-time section for CCF averaged between 88° to 92°E to highlight the time evolution of topographically influenced CCF. The left-hand figure shows the surface altitude averaged over the same longitudes. Small values of CCF are observed over the TP from 9 to 12 LST. CCF increases after 13 LST over mountain ranges C and D, reaching a maximum at 17–18 LST over the summits. A CCF maximum also develops over the mountain range along 34°N (the Tanggula Range), although CCF there is smaller than over C and D. Subsequently, areas of high CCF move from the two mountain ranges and merge over valley B, remaining there between 19 and 06 LST. Relatively high values of CCF also persist until 06 LST over the bottom of valley A. A valley-mountain contrast is distinct over the southern TP.

Figure 2b is similar to Fig. 2a, but for rainfall frequency (RF). Features in the diurnal variation show contrasts between mountain ranges and valleys that are similar to variations in CCF. RF reaches a maximum over mountain ranges C and D around 17 LST, after which time RF decreases rapidly although high clouds still persist. In valley B, RF peaks between 20 and 22 LST and persists until 03 LST, like CCF. Daytime precipitation starts a few hours earlier than high cloud over the plateau except in the valley bottoms.

Diurnal variations in PW have been observed by GPS at Lhasa during the pre-monsoon and monsoon (Takagi et al. 2000). During the summer monsoon, PW decreases from morning until 15 LST and then increases until 21 LST. Subsequently, PW is nearly constant until 03 LST when it decreases. Such an evolution is consistent with the CCF and RF sequence over valley B.

Figure 3 shows a typical diurnal variation to illustrate the evolution of convection during the transition phase from afternoon to night. Figure 3a shows the *Ic* distribution at 15 LST (09UTC) on 13 August 1998. Meso-β scale (a few tens of kilometers) convective clouds develop along mountain ranges C and D. Convection grows and merges so that by 18 LST (12UTC), convection is centered over the mountains. Some new convective cells evolve to larger cells over valley B as the valley-mountain contrast becomes ambiguous. At 19 LST (Fig. 3c), high clouds cover the southern TP, and there are some enhanced convective cells. Convective cells with scales of about 100 km are over valley region B by 21 LST (15 UTC). One cell near 30°N, 90.5°E at 18 LST moves southeastward and develops near 29.5°N,

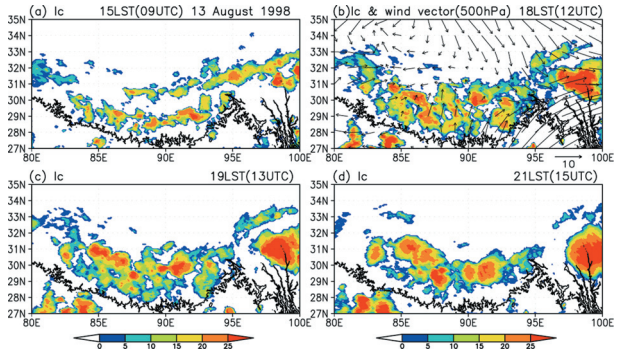

Fig. 3. *Ic* distribution at (a) 15 LST, (b) 18 LST, (c) 19 LST, and (d) 21 LST on 13 August 1998. Wind vectors at 500 hPa are shown in (b). The reference arrow is 10 m s^{-1}. The thick solid line denotes the 3000-m topographic contour.

91.5°E at 21 LST. A second cell near 29.5°N, 88°E develops in place over valley B. These convective cells remain nearly stationary until 02 LST (20 UTC) (not shown). Wind fields over the southern TP are characterized by weak southerlies at 500 hPa (Fig. 3b) and weak westerlies (<~10 m s^{-1}) at 200 hPa (not shown). Weak ambient winds over the TP are consistent with an atmospheric environment there that favors the development of thermally driven local circulations.

Figure 4a shows mean 6-hour RF and total 6-hour near-surface rainfall averaged between 88° and 92°E and between 12–18 LST (06–12UTC) for five years (1998–2002). Gray bars indicate total precipitation, while black bars denote total convective rainfall. The difference between the two bars represents the amount of stratiform rain. High RF occurs over mountain ranges C and D. Large precipitation totals (exceeding 2 mm in 6 hours) occurred over the mountain ranges. On average, convective rains account for more than 60 percent of the afternoon precipitation over mountain ranges, although stratiform rainfall amounts dominate at some locations even in the mountains. RF is low over valley B between 12–18 LST. In contrast, between 18 and 24 LST (12–18 UTC), RF is high over valley B, where precipitation exceeds 2 mm $(6\ hr)^{-1}$. During these hours, convective rains deposit more than half of the total precipitation over the valley bottom.

Shimizu et al. (2001) used TRMM PR data in the summer of 1998 to show that precipitation associated with deep convection develops between 15 and 18 LST over the central TP (valley A). In contrast, stratiform precipitation intensity peaks between 18 and 24 LST. Comparison between Figs. 4a and 4b suggests that, on average, convective rains prevail more during the day than at night. Convective rains remain more common at night over the bottom of the major valleys. However, stratiform rains do become more common at night than during the day.

Figure 5 shows the spatial evolution of 6-hour total precipitation. The distribution of precipitation during the day (Fig. 5a) and at night (Fig. 5b) is consistent with CCF distributions (Figs. 1b and c, respectively). During the day, heavier rains (>2.0 mm per 6 hours) correspond well with mountain ranges C and D; less precipitation falls in valley B. Heavy rains also fall over the southeastern TP (around 30°N, 98°E). In contrast, heavier rain occurs at night in valley B.

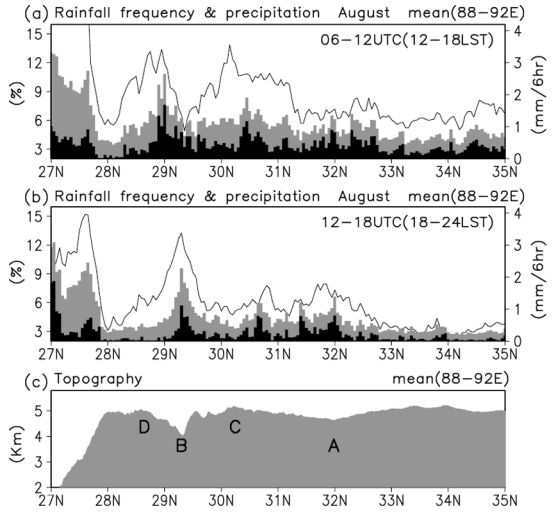

Fig. 4. (a) Mean 6-hour rainfall frequency (solid line, left axis) and integrated 6-hour precipitation (gray bar; right axis) averaged for five Augusts (1998–2002) and between 88° and 92°E for 12–18 LST. Black bar indicates the amount of convective-type rain. (b) As in (a) but for 18–24 LST. (c) Topography averaged between 88° and 92°E.

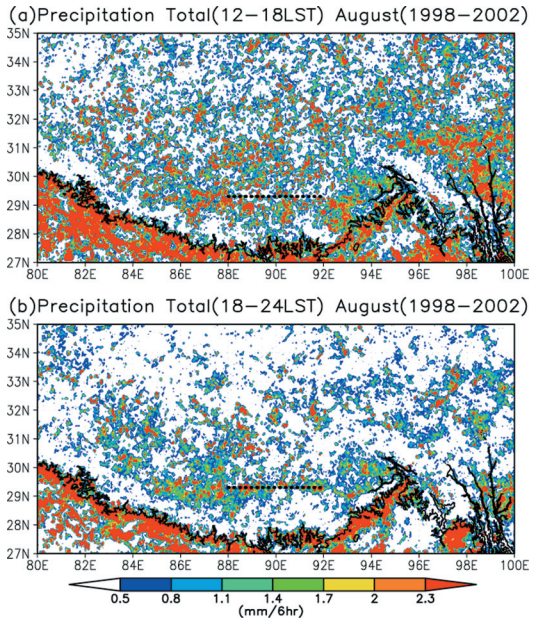

Fig. 5. Spatial distribution of 6-hour total near-surface rainfall (a) from 12 to 18 LST and (b) from 18 to 24 LST. The dotted line indicates valley B (Yarlung-Zangbo River). The thick solid line is the 3000-m topographic contour.

4. Discussion

High clouds are common over the southern TP during the mature phase of the summer monsoon. Uyeda et al. (2001) showed that convection in the central TP can reach the tropopause during the monsoon because the ambient wind is weaker than during

the pre-monsoon season. In August 1998, a core of the Asian subtropical jet was at 40°N at 200 hPa. Weak ambient winds (<10 m s^{-1}) from the surface to 200 hPa occurred over the areas between 28° and 31°N, where high clouds were enhanced (not shown). The atmospheric structure there allowed convection to reach the upper troposphere.

The atmospheric structure also supported thermally induced local circulations. Afternoon convection over the mountain ranges suggests convergence induced by a local circulation (Kuwagata and Kimura 1997). The meridional width (~150 km) and depth (~1,000 m) of valley B are similar to the most effective topographic scales for water transport (160 km width and 1000 m depth) shown in Kuwagata et al. (2001). Characteristic valley scales over the southern TP efficiently trigger afternoon moist convection over the mountain ranges.

Active convection and precipitation increased after sunset in valley B. Dynamic lifting is necessary to initiate convection. A possible trigger for nocturnal convection is low-level convergence of down-slope flow from mountain ranges C and D. Surface cooling could cause such a flow. Cold outflow from deep precipitating convection over the mountains may strengthen low-level convergence over valley B. Yang et al. (2004) showed that convergence between pre-existing up-slope flow and down-slope flow forced by evaporative cooling of precipitation over the mountain could trigger deep convection that would subsequently propagate from mountain to valley in the central TP. Valley B (the Yarlung-Zangbo River) is aligned roughly east-west, merging with the Brahmaputra valley east of 94°E. Moisture transport associated with a wind system flowing along the Brahmaputra to valley B may enhance convection.

The formation and development of convective-type clouds and phase differences in the diurnal cycle over the southern TP are strongly influenced by mountain-valley terrain. Thermally induced mountain-valley circulations help regulate active convection over the TP in summer. However, the effect of a plateau-scale diurnal circulation system cannot be neglected in a detailed description of the diurnal convective cycle. A plateau-scale circulation may enhance southerly moisture inflow towards the TP. Such a moisture inflow helps to maintain high specific humidity and a convectively unstable stratification over the southern TP. Further study will reveal interactions between plateau-scale and regional-scale circulation systems and how they influence the diurnal cycle of convection over the southern TP in summer.

5. Conclusion

This study examined characteristics of the diurnal cycle in convection and precipitation over the complex mountain-valley terrain over the southern TP in August. Special attention was given to the evolution between noon and midnight.

Cloud-cover frequency (CCF) for high cloud increased after 13 LST (07 UTC) over the mountain ranges along 28.5°N and 30.2°N, reaching a maximum near 18 LST (12 UTC). High values of CCF subsequently moved over the valley along 29.3°N. Relatively large CCF persisted over the valley until early morning. A similar evolution occurred in rainfall frequency derived from TRMM PR.

Over the TP as a whole, the ratio of convective-type rain to total rainfall is larger during the day (12–18 LST) than at night (18–24 LST). However, mesoscale convective systems are common over major valleys at night.

Acknowledgements

We thank Dr. K. Ueno of the University of Shiga Prefecture for his helpful comments. The authors thank Mr. H. Ichikawa of Nagoya University for processing TRMM PR data. Dr. T. Kikuchi of Kochi University provided GMS-IR data.

References

Awaka, J., T. Iguchi, H. Kumagai and K. Okamoto, 1997: Rain type classification algorithm for TRMM precipitation radar. *Proc. IGARSS'97*, IEEE, Singapore, 1633–1635.

Fujinami, H., and T. Yasunari, 2001: The seasonal and intraseasonal variability of diurnal cloud activity over the Tibetan Plateau. *J. Meteor. Soc. Japan*, **79**, 1207–1227.

Kurosaki, Y., and F. Kimura, 2002: Relationship between topography and daytime cloud activity around Tibetan Plateau. *J. Meteor. Soc. Japan*, **80**, 1339–1355.

Kuwagata, T., and F. Kimura, 1997: Daytime boundary layer evolution in a deep valley. Part II: Numerical simulation of the cross-valley circulation. *J. Appl. Meteor.*, **36**, 883–895.

Kuwagata, T., A. Numaguti and N. Endo, 2001: Diurnal variation of water vapor over the central Tibetan Plateau during summer. *J. Meteor. Soc. Japan*, **79**, 401–418.

Murakami, M., 1983: Analysis of the deep convective activity over the western Pacific and Southeast Asia. Part I: Diurnal variation. *J. Meteor. Soc. Japan*, **61**, 60–76.

Sasaki, T., P. Wu, F. Kimura, T. Yoshikane and J. Liu, 2003: Drastic evening increase in precipitable water vapor over the southeastern Tibetan Plateau, *J. Meteor. Soc. Japan*, **81**, 1273–1281.

Shimizu, S., K. Ueno, H. Fujii, H. Yamada, R. Shirooka and L. Liu, 2001: Mesoscale characteristics and structures of stratiform precipitation on the Tibetan Plateau. *J. Meteor. Soc. Japan*, **79**, 435–461.

Takagi, T., F. Kimura and S. Kono, 2000: Diurnal variation of GPS precipitable water at Lhasa in premonsoon and monsoon periods. *J. Meteor. Soc. Japan*, **78**, 175–180.

Ueno, K., 1998: Characteristics of plateau-scale precipitation in Tibet estimated by satellite data during 1993 monsoon season. *J. Meteor. Soc. Japan*, **76**, 533–548.

Ueda, H., H. Kamahori and N. Yamazaki, 2003: Seasonal contrasting features of heat and moisture budgets between the eastern and western Tibetan Plateau during the GAME IOP. *J. Climate*, **16**, 2309–2324.

Uyeda, H., H. Yamada, J. Horikomi, R. Shirooka, S. Shimizu, L. Liu, K, Ueno, H. Fujii and T. Koike, 2001: Characteristics of convective clouds observed by a Doppler radar at Naqu on the Tibetan Plateau during the GAME-Tibet IOP. *J. Meteor. Soc. Japan*, **79**, 463–474.

Yamazaki, N., H. Kamahori, A. Yatagai, K. Takahashi, H. Ueda, K. Aonashi, K. Kuma, Y. Takeuchi, H. Tada, Y. Fukutomi, H. Igarashi, H. Fujinami and Y. Kajikawa, 2000: Release of GAME reanalysis data. *Tenki*, **47**, 659–663. (in Japanese).

Yanai, M., C. Li and Z. Song, 1992: Seasonal heating of the Tibetan Plateau and its effects on the evolution of the Asian summer monsoon. *J. Meteor. Soc. Japan*, **70,** 319–351.

Yanai, M., and C. Li, 1994: Mechanism of heating and the boundary layer over the Tibetan Plateau, *Mon. Wea. Rev.*, **122**, 305–323.

Yang, K., T. Koike, H. Fujii, T. Tamura, X. Xu, L.Bian and M. Zhou, 2004: The daytime evolution of the atmospheric boundary layer and convection over the Tibetan Plateau: Observations and simulations, *J. Meteor. Soc. Japan*, **82**, 1777–1792.

(*Manuscript received 12 January 2005, accepted 1 April 2005*)